Efficiency Optimization of a 100-W, 500 000-rpm Permanent-Magnet Machine Including Air Friction Losses

J. Luomi
Power Electronics Laboratory
Helsinki University of Technology
FI-02150 TKK, Finland
jorma.luomi@tkk.fi

C. Zwyssig, A. Looser, and J.W. Kolar
Power Electronic Systems Laboratory
ETH Zurich
CH-8092 Zurich, Switzerland
zwyssig@lem.ee.ethz.ch

Abstract — **This paper proposes a method for the efficiency optimization of ultra-high-speed permanent-magnet machines. Analytical methods are applied for the modeling of the machine that is equipped with a diametrically magnetized rotor and a slotless stator. The outer dimensions of the machine are design constraints, and the internal dimensioning is optimized for minimum losses. The air friction losses are taken into account in addition to the usual iron losses, copper losses, and eddy current losses. Laminated silicon iron or laminated amorphous iron is used as the stator core material. The results show that air friction losses influence the optimum design considerably, leading to a small rotor diameter at high speeds. The loss minimization and the amorphous iron core make it possible to reduce the calculated losses by 63% as compared to a machine design not considering air friction losses. The resulting efficiency is 95% for a 100-W, 500 000-rpm machine excluding bearing losses.**

I. Introduction

Development of ultra-high-speed electrical drive systems is needed for new emerging applications, such as generators/starters for micro gas turbines, turbo-compressor systems, drills for medical applications, and spindles for machining. Typically, the power ratings of these applications range from a few watts to a few kilowatts, and the speeds from a few tens of thousands rpm up to a million rpm [1]. Recently, a 100-W, 500 000-rpm permanent-magnet (PM) machine has been designed and investigated experimentally [2], [3]. For such high speeds, the mechanical rotor construction and the minimization of high-frequency losses are the main challenges. This machine has a diametrically magnetized cylindrical Sm_2Co_{17} permanent magnet encased in a titanium sleeve for sufficiently low mechanical stresses on the magnet. The slotless stator core consists of 168-µm silicon-iron laminations, and the three-phase air-gap winding is made of litz wire with 0.071 mm strands for low copper losses. The cross-section of the machine is illustrated in Fig. 1.

In designing an ultra-high-speed machine, it is important to optimize the efficiency—i.e. minimize the losses—when the outer dimensions of the machine are design constraints. Previously, such optimizations have been based on resistive losses in the stator winding and iron losses in the stator core [4] and, in addition, eddy current losses in the rotor [5]. However, air friction losses are an important part of the total losses in an ultra-high-speed machine [2]. Therefore, these losses should also be taken into account in the optimization.

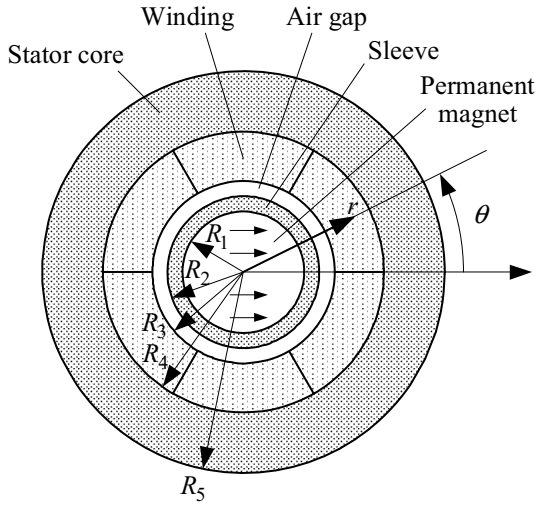

Figure 1. Machine cross-section and symbol definitions: diametrically magnetized cylindrical permanent magnet rotor inside a slotless stator.

This paper proposes a method for the loss minimization of ultra-high-speed PM machines including air friction losses. Analytical methods are applied for the modelling. In the following, models are first presented for the magnetic field and the loss components. Then, the optimization procedure is briefly described and, finally, results of the loss minimization are shown.

II. Magnetic Field and Torque

A solution of the magnetic field is needed for analyzing the operating point, resistive losses, eddy current losses, and iron losses. Today, numerical analysis based on the finite-element (FE) method is the standard methodology for such calculations. However, analytical models can give more insight into the problem, they are in many cases computationally efficient, and result in smooth solutions, which is favourable in optimization. Analytical solutions of the magnetic field have been derived for permanent-magnet machines with radially magnetized magnets

0197-2618/07/$25.00 © 2007 IEEE

in the rotor, e.g., [6], [7]. Solutions for machines with diametrically magnetized rotors have been presented in [8], [9].

Usually, the permeability of the stator iron core has been assumed infinite when the magnetic field of a permanent-magnet machine is solved analytically, and the solution is restricted to the air gap and the rotor. However, an analytical model of the magnetic field in the stator core can be used for the evaluation of the iron loss distribution [10]. In the following, a solution of the magnetic field is derived for the entire cross-section of the machine, including the cylindrical stator core.

A. Problem Formulation

The cross section of the two-pole machine is illustrated in Fig. 1. The symbols for the radial dimensions are: radius of the permanent magnet R_1; outer radius of the rotor sleeve R_2; inner radius of the stator winding R_3; and inner and outer radii of the stator core R_4 and R_5, respectively. The length of the stator core is denoted by L, and the air gap is $\delta = R_3 - R_2$.

A two-dimensional boundary value problem is formulated for the magnetic field, and the effects of the third dimension are ignored. The polar $r-\theta$ coordinate system fixed to the rotor cross-section is illustrated in Fig. 1. The diametrically magnetized permanent magnet has a uniformly distributed remanence flux density $\boldsymbol{B}_{rem}$ in the direction of $\theta = 0$. The magnetic flux density is given by

$$\boldsymbol{B} = \mu_0 \boldsymbol{M}_p + \mu_r \mu_0 \boldsymbol{H} \tag{1}$$

where $\boldsymbol{M}_p$ is the permanent magnetization, $\boldsymbol{H}$ is the magnetic field strength, and μ_r is the relative recoil permeability.

The problem region is divided into three subregions. In the permanent magnet region ($0 \le r \le R_1$), $\boldsymbol{M}_p = \boldsymbol{B}_{rem}/\mu_0$ and $\mu_r = \mu_{r1}$. The uniform permanent magnetization is given by

$$\boldsymbol{M}_p = \mathbf{u}_r M_p \cos\theta - \mathbf{u}_\theta M_p \sin\theta \tag{2}$$

where $\mathbf{u}_r$ and $\mathbf{u}_\theta$ are the radial and azimuthal unit vectors, respectively. In the non-ferromagnetic region between the permanent magnet and the stator core ($R_1 < r < R_4$), $\boldsymbol{M}_p = 0$ and $\mu_r = 1$. In the stator core ($R_4 < r < R_5$), $\boldsymbol{M}_p = 0$ and $\mu_r = \mu_{r5}$.

The magnetic field is modelled by means of the magnetic scalar potential ϕ defined by $\boldsymbol{H} = -\nabla\phi$. Inserting this definition with (1) into the governing equation $\nabla \cdot \boldsymbol{B} = 0$ yields the Laplace equation $\nabla^2\phi = 0$ for the scalar potential. It is to be noted that $\nabla \cdot \boldsymbol{M}_p = 0$ for uniform permanent magnetization.

In the polar coordinate system, the partial differential equation of the scalar potential is

$$\frac{\partial^2\phi}{\partial r^2} + \frac{1}{r}\frac{\partial\phi}{\partial r} + \frac{1}{r^2}\frac{\partial^2\phi}{\partial\theta^2} = 0 . \tag{3}$$

In addition to the partial differential equation, interface and boundary conditions are needed. The continuity of the tangential component of the magnetic field strength requires that ϕ is continuous over the interfaces at R_1 and R_4. The continuity of the normal component of the magnetic flux density requires that $M_p \cos\theta - \mu_r \partial\phi/\partial r$ is continuous over the interfaces at R_1 and R_4. The normal component of the magnetic flux density vanishes at the outer boundary of the machine, which gives the boundary condition $-\mu_r \partial\phi/\partial r = 0$ at R_5.

B. Magnetic Field Solution

Expressions for the magnetic field are obtained in the whole machine by solving the problem consisting of the partial differential equation (3) and the interface and boundary conditions. The solution can be obtained by separation of variables. In the permanent magnet ($0 \le r \le R_1$), the radial and azimuthal components of the magnetic flux density are

$$B_r = K_{B1}\cos\theta ; \; B_\theta = -K_{B1}\sin\theta \tag{4}$$

respectively, where the flux density coefficient is

$$K_{B1} = \frac{B_{\mathrm{rem}}}{N}\left[\left(1-\frac{R_4^2}{R_5^2}\right)\left(1+\frac{R_1^2}{R_4^2}\right)+\frac{1}{\mu_{\mathrm{r3}}}\left(1+\frac{R_4^2}{R_5^2}\right)\left(1-\frac{R_1^2}{R_4^2}\right)\right] \tag{5}$$

with the definition

$$\begin{aligned} N = {} & \left[1-\left(\frac{R_4}{R_5}\right)^2\right]\left[(\mu_{r1}+1)-(\mu_{r1}-1)\left(\frac{R_1}{R_4}\right)^2\right] \\ & + \frac{1}{\mu_{\mathrm{r5}}}\left[1+\left(\frac{R_4}{R_5}\right)^2\right]\left[(\mu_{r1}+1)+(\mu_{r1}-1)\left(\frac{R_1}{R_4}\right)^2\right] . \end{aligned} \tag{6}$$

In the non-ferromagnetic region ($R_1 \le r \le R_4$), the radial and azimuthal components of the magnetic flux density are

$$B_r = K_{B2}\left[1+\left(\frac{R_4}{r}\right)^2\right]\cos\theta ; \; B_\theta = -K_{B2}\left[1-\left(\frac{R_4}{r}\right)^2\right]\sin\theta \tag{7}$$

respectively, where the flux density coefficient is

$$K_{B2} = \frac{B_{rem}}{N}\left\{\left[1-\left(\frac{R_4}{R_5}\right)^2\right]-\frac{1}{\mu_{\mathrm{r5}}}\left[1+\left(\frac{R_4}{R_5}\right)^2\right]\right\}\left(\frac{R_1}{R_2}\right)^2 . \tag{8}$$

In the stator core ($R_4 \le r \le R_5$), the components of the magnetic flux density are

$$B_r = K_{B3}\left[-1+\left(\frac{R_5}{r}\right)^2\right]\cos\theta ; \; B_\theta = -K_{B3}\left[1+\left(\frac{R_5}{r}\right)^2\right]\sin\theta \tag{9}$$

respectively, where the flux density coefficient is

$$K_{B3} = \frac{2B_{rem}}{N}\left(\frac{R_1}{R_5}\right)^2 . \tag{10}$$

The magnetic field component caused by the stator current can also be included in the analytical model in a fashion similar to [11]. However, the magnetic field of a machine with an air-gap winding is mainly produced by the permanent magnet, and the influence of the stator winding is small [3]. Hence the efficiency optimization can be carried out without modelling the magnetic field component caused by the stator current.

C. Comparison with Finite Element Solution

Fig. 2 shows a comparison between the flux densities obtained using the analytical model and a FE method, respectively. The results agree well with each other. FE analysis is needed only if magnetic saturation occurs. However, it is typical of ultra-high-speed PM machines with a slotless design that the magnetic flux density does not reach values causing magnetic saturation in the iron core.

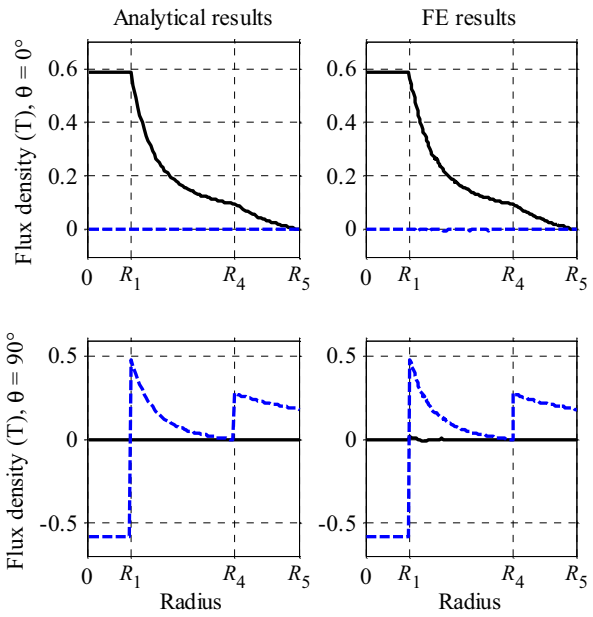

Figure 2. Comparison between analytical and FE solutions. Radial flux density components are plotted as solid lines, azimuthal components as dashed lines. $B_{rem} = 1.1$ T, $\mu_{r1} = 1.05$, $\mu_{r5} = 1000$, $R_5 = 8$ mm, $R_4 = 5.6$ mm, and $R_1 = 1.68$ mm.

D. Torque Calculation

The density of the azimuthal force component caused by the spatial fundamental wave J_1 of the current density in the stator winding is $J_1 B_r$. The electromagnetic torque is obtained as the integral

$$T_e = L \int_{-\pi}^{\pi} \int_{R_3}^{R_4} r^2 J_1 B_r \, dr d\theta \,. \tag{11}$$

The stator current component in the direction of the permanent-magnet flux is controlled to zero. Using (7), the integration in (11) results in

$$T_e = \sqrt{2}\pi k_w k_{Cu} J K_{B2} L R_4^3 \left(\frac{4}{3} - \frac{R_3}{R_4} - \frac{1}{3} \frac{R_3^3}{R_4^3} \right) \tag{12}$$

where k_w is the fundamental-wave winding factor, k_{Cu} is the winding fill factor and J the rms current density in the conductors.

The current density J can be solved from (12) if the electromagnetic torque is known for an operating point. The winding factor for the distributed three-phase air-gap winding shown in Fig. 1 is

$$k_w = \frac{6}{\pi} \sin \frac{\pi}{6} \,. \tag{13}$$

III. Loss Models

A. Copper Losses

The frequency of the stator current is high (8.3 kHz in the 500 000 rpm machine). Therefore, eddy currents increase the copper losses of the stator winding. In addition to the stator current, the air-gap flux causes considerable eddy-current losses in the winding due to the slotless design of the stator. In order to reduce the losses, the winding is made of litz wire.

The copper losses consist of the current dependent resistive losses $P_{Cu,s}$ in the stator winding, which include the influence of the skin effect, and of the proximity effect losses $P_{Cu,p}$, which are mainly due to the eddy currents induced by the magnetic field of the permanent magnet. The copper losses are

$$P_{Cu} = P_{Cu,s} + P_{Cu,p} = I^2 F + G \frac{\hat{H}^2}{\sigma} \tag{14}$$

where I is the rms stator current, $\hat{H}$ is the peak magnetic field strength in the winding, and σ is the conductivity of the conductors. The coefficients F and G include the effects of the eddy currents, and are calculated based on the frequency, the conductivity, and the geometry of the winding arrangement.

There are various commonly used methods for calculating the coefficients in (14). The Ferreira method [12] was chosen for the analysis. At significantly higher frequencies or larger strand diameters, the accuracy could be increased by using a method based on function fitting for the calculation of the proximity effect losses [13].

B. Iron Losses

The iron losses are calculated as an integral over the iron volume V_{Fe} using the Steinmetz equation,

$$P_{Fe} = \int_{V_{Fe}} C_m \cdot f^{\alpha} \cdot \hat{B}^{\beta} \, dV \tag{15}$$

where f is the frequency and $\hat{B}$ the peak magnetic flux density. The coefficients C_m, α and β are taken from manufacturer's data sheets.

C. Air Friction Losses

For simple geometries, such as cylinders and disks, air friction losses can be calculated analytically with friction coefficients based on empirical data [14]. In the following, only the air gap is taken into account in the calculation of the air friction losses, and the losses at the end caps are omitted.

The air friction losses of a long rotating cylinder encased in a stationary hollow cylinder are

$$P_{f,air} = c_f \pi \rho_{air} \omega^3 R_2^4 L \tag{16}$$

where ρ_{air} is the density of the air, ω the angular speed, R_2 the radius, and L the length of the cylinder. The friction coefficient c_f depends on the radius of the cylinder, the air gap δ, and the Reynolds number and the Taylor number, which are defined as

$$Re = \frac{R_2^2 \omega}{\nu}; \qquad Ta = \frac{R_2 \omega \delta}{\nu} \sqrt{\frac{\delta}{R_2}} \tag{17}$$

where ν is the kinematic viscosity of air. The flow stability depends on the Taylor number; the flow can be divided into laminar Couette flow ($Ta < 41.3$), laminar flow with Taylor vortices ($41.3 < Ta < 400$), and turbulent flow ($Ta > 400$).

For laminar Couette flow, the friction coefficient can be determined analytically, but measurements show discrepancies with the theoretical values. Therefore, empirical data is usually used, and correction factors are applied to adapt for different

geometries [14]. For the air gap of the machine under investigation, the friction coefficient

$$c_f = \frac{1.8}{Re}\left(\frac{\delta}{R_2}\right)^{-0.25}\frac{R_3^2}{R_3^2 - R_2^2} \tag{18}$$

can be used. Beyond the transition point from laminar flow to flow with Taylor vortices, measurements show a friction coefficient

$$c_f \propto Ta^{-0.2}. \tag{19}$$

This model for air friction losses was experimentally validated in [2].

D. Other Losses and Shaft Torque

The eddy-current losses in the rotor of a slotless PM machine are generally very low as shown in [5]. Therefore, the rotor losses are ignored in the following. Furthermore, it is to be noted that the bearing losses are not considered in the efficiency optimization of the machine since they are usually more dependent on the application than on the inner dimensions of the motor.

The machine is to be optimized for a given mechanical shaft torque T_m. When the proximity effect losses, iron losses, and air friction losses are taken into account, the electromagnetic torque can be calculated by

$$T_e = T_m + \frac{P_{Cu,p} + P_{Fe} + P_{f,air}}{\omega}. \tag{20}$$

IV. Mechanical Model

A two-dimensional mechanical model is used for the rotor. The stresses of the rotor construction with the permanent-magnet shrink-fitted into a titanium sleeve have been analyzed in [3]. The following specifications have to be fulfilled in the entire operation region:

- The torque transfer and low eccentricity are guaranteed by allowing no lift-off of the sleeve. Thus the radial stress at the interface between the permanent magnet and the sleeve has to be negative, which is most critical at the maximum speed.
- Stresses in the entire permanent magnet have a safety margin of 30% to the tensile strength of Sm_2Co_{17} (120 MPa). The most critical stress occurs at the maximum speed in the centre of the magnet.
- Stresses in the entire sleeve have a safety margin of 50% to the tensile strength of titanium (900 MPa). The most critical stress occurs at the maximum speed on the inner side of the sleeve.
- The sleeve has a minimum thickness (0.25 mm) for manufacturability reasons.

V. Optimization

A. Loss Minimization

The goal is to minimize the total losses obtained from (14)–(16), i.e. the objective function is

$$P_d = P_{Cu} + P_{Fe} + P_{f,air}. \tag{21}$$

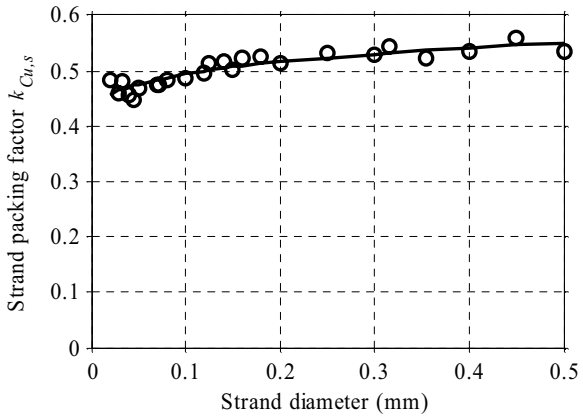

Figure 3. Strand packing factor $k_{Cu,s}$ as function of strand diameter: manufacturer's data (markers) and fitted curve (line).

The losses are minimized for a given rotational speed n and shaft torque T_m. The outer radius R_5 and length L of the stator core are kept constant, and the independent variables are the magnet radius R_1, the air gap δ, and the inner radius of the stator core R_4.

The loss minimization is constrained in order to obtain a geometrically, mechanically, and magnetically feasible design. The sleeve thickness $R_2 - R_1$ is kept at the minimum value given by the mechanical analysis. The minimum value for the air gap δ is 0.2 mm, and the minimum value for the thickness of the stator core ($R_5 - R_4$) is 1 mm. In addition, the flux density in the iron core is limited to a maximum value (1.3 T for a silicon iron stack and 1.1 T for an amorphous iron stack). In the results presented in this paper, a constant temperature of 120ºC is assumed for the stator winding.

Many different methods can be used for solving the minimization problem. A straightforward choice is the Nelder-Mead simplex method included in the MATLAB software as the function fminsearch. The constraints can be included in this derivative-free minimization method by giving the objective function a high value if the design is not feasible.

B. Litz Wire Optimization

The strand diameter of the litz wire influences only the copper losses. During the loss minimization, the strand diameter giving the lowest copper losses is selected for every feasible design. Making the strands thinner decreases the eddy currents, but increases the resistive losses if the winding fill factor decreases.

The winding fill factor is given by

$$k_{Cu} = k_{Cu,t} k_{Cu,s}. \tag{22}$$

Here, the turn fill factor k_{Cu} is defined as the ratio of the area occupied by the litz wires to the total cross-sectional area of the winding. The strand packing factor $k_{Cu,s}$ is the ratio of the copper area of the strands in the wire to the area of the wire. The turn fill factor is assumed to be constant, whereas the strand packing factor is a function of the strand diameter. Fig. 3 shows the strand packing factors $k_{Cu,s}$ for various strand diameters obtained from manufacturer's data [15].

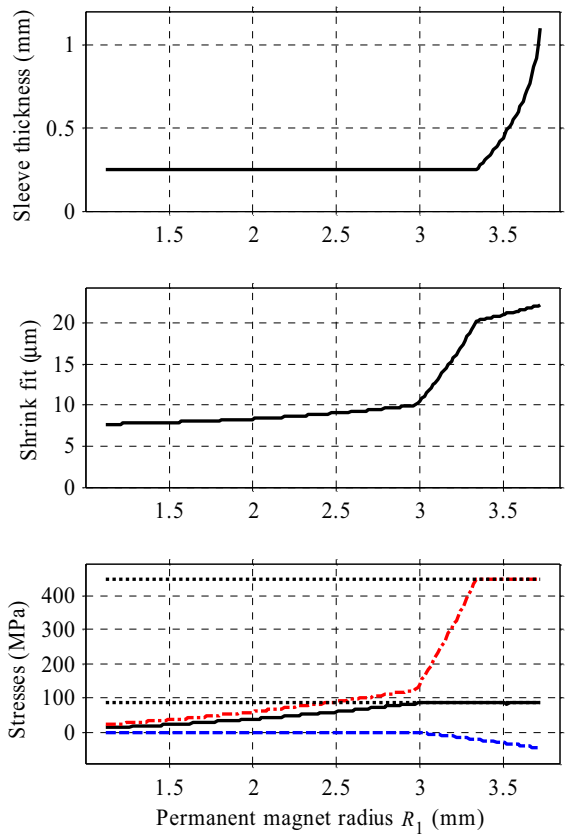

Figure 4. Results of mechanical analysis as function of rotor radius at 500 000 rpm. The first subfigure shows the sleeve thickness $R_2 - R_1$, the second subfigure shows the shrink fit, and the third subfigure shows the radial stress in the center of the permanent magnet (solid), the radial stress at the interface (R_1) (dashed), the tangential stress in the sleeve at R_1 (dash-dotted), and stress limits in the magnet and sleeve (dotted).

TABLE I
PARAMETERS

Symbol	Quantity	Value
Permanent magnet		
B_{rem}	Remanence flux density	1.1 T
μ_{r1}	Relative recoil permeability	1.05
Silicon-iron laminations (168 µm)		
μ_{r5}	Relative permeability	1860
C_m	Steinmetz coefficient	21.8 W/m^3
α	Steinmetz coefficient	1.42
β	Steinmetz coefficient	1.50
Amorphous iron (Metglas magnetic alloy 2605SA1)		
μ_{r5}	Relative permeability	35100
C_m	Steinmetz coefficient	0.94 W/m^3
α	Steinmetz coefficient	1.53
β	Steinmetz coefficient	1.72
Air		
ρ_{air}	Density	1.29 kg/m^3
ν	Kinematic viscosity	0.000014 m^2/s

VI. RESULTS

A. Mechanical Rotor Model

The thickness of the rotor sleeve and the interference fit needed were calculated using the mechanical model. The results are shown in Fig. 4 for a rotor with a maximum speed of 500 000 rpm. For small rotor radii, the sleeve thickness is at the minimum value defined by the manufacturability; the shrink fit ensures that the sleeve does not lift off. At 3 mm magnet radius, the stress in the magnet reaches its limit, and the shrink fit has to be enforced to guarantee the safety margin to the tensile strength of Sm_2Co_{17}. At 3.3 mm, the stress in the titanium sleeve reaches its limit, and the sleeve thickness has to be increased in order to guarantee the safety margin to the tensile strength of titanium.

B. Fixed Outer Dimensions

The parameters used in the efficiency optimization are given in Table I. Figs. 5 and 6 illustrate the dependence of the losses on the internal radial dimensions of the machine. The outer dimensions of the existing machine were used ($R_5 = 8$ mm and $L = 15$ mm), and the stator core material was laminated silicon iron. The sleeve thickness was fixed to the original value (0.5 mm), and so was the air gap (0.5 mm) and the strand diameter of the litz wire (0.071 mm). In Fig. 5, the total losses are plotted as a function of the magnet radius R_1 for various values of the inner radius R_4 of the stator core. The individual loss components are shown in Fig. 6 for the original value $R_4 = 5.5$ mm. It can be seen that the total losses depend strongly on the radius of the permanent magnet, whereas the sensitivity to the inner diameter of the core is low if the radius of the permanent magnet is appropriately chosen.

The minimum of the losses is about 9 W, and it is obtained at $R_4 = 5.3$ mm and $R_1 = 1.7$ mm. The original machine design is based on the values $R_4 = 5.5$ mm and $R_1 = 2.5$ mm [3], and it has 14.2 W of losses. Thus a reduction of losses by 5.2 W can be obtained by changing the internal radial dimensions of the machine.

It can be seen that the copper losses of the optimized machine are higher than those of the existing machine, but the air friction and iron losses are reduced. A smaller magnet radius leads to a lower air-gap flux density and thus increases the copper losses. However, a larger amount of air friction and iron losses can be avoided by decreasing the magnet radius.

The losses of the existing machine obtained with the loss models presented in this paper are shown by circular markers in Figs. 5 and 6. There are small differences between the values shown here and the ones obtained in [2] by means of measurements and separation of losses; these differences originate from the less accurate model used earlier for iron losses and from a small difference in the winding geometry and temperature.

C. Variable Outer Dimensions and Strand Diameter

For an improved loss minimization, the sleeve thickness was reduced to the minimum value given by the mechanical analysis ($R_2 - R_1 = 0.25$ mm), and the optimization was based on the three independent variables (R_1, δ, and R_4). In addition, the strand diameter giving lowest copper losses was determined for the litz wire. In all the following examples, the

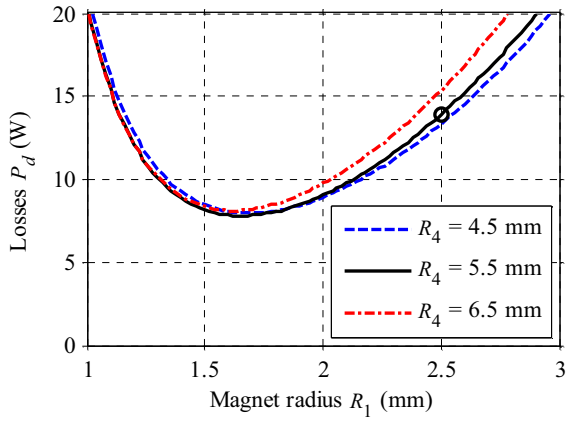

Figure 5. Losses of the machine with fixed outer dimensions of the stator core ($R_5 = 8$ mm , $L = 15$ mm) and a shaft power of 100 W at a rotational speed of 500 000 rpm for variable magnet radius R_1 and various values of the inner radius R_4 of the stator core. The circle shows the value for the existing machine with $R_4 = 5.5$ mm and $R_1 = 2.5$ mm [3].

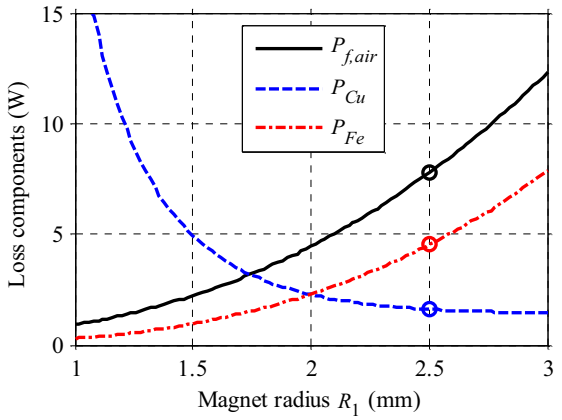

Figure 6. Loss components of the machine with fixed outer dimensions of the stator core ($R_5 = 8$ mm , $L = 15$ mm) and a shaft power of 100 W at a rotational speed of 500 000 rpm for variable magnet radius R_1 and constant inner radius of the stator core, $R_4 = 5.5$ mm . The circle shows the values for the existing machine with $R_1 = 2.5$ mm [3].

loss minimization resulted in an air gap value of $\delta = 0.2$ mm , i.e. the minimum value. The optimum strand diameter of the litz wire varied between 0.03 and 0.05 mm, but the influence of small changes in the strand diameter is insignificant since the proximity effect losses are much lower than the other loss components.

Fig. 7 shows the magnet radius R_1 and inner radius R_4 of the stator core for the laminated silicon iron core material. The results are shown for variable outer radius R_5 of the stator core and various values of the core length L . The corresponding total losses are shown in Fig. 8. For the original outer dimensions ($R_5 = 8$ mm and $L = 15$ mm), the losses can be reduced to about 7 W by choosing $R_4 = 5.1$ mm and $R_1 = 1.8$ mm . Thus the reduction of the air gap and sleeve thickness allows a loss reduction by 2 W from the result shown in Fig. 5. The losses can be further reduced by increasing the outer dimensions of the machine.

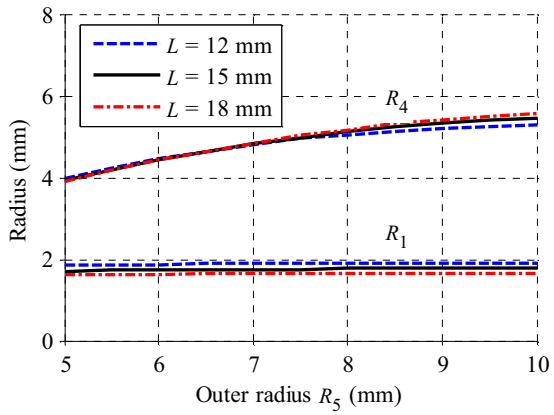

Figure 7. Optimization results for the silicon iron core: magnet radius R_1 and inner radius R_4 of the stator core for variable outer radius R_5 of the stator core and various values of the core length L . The shaft power is 100 W and the rotational speed 500 000 rpm.

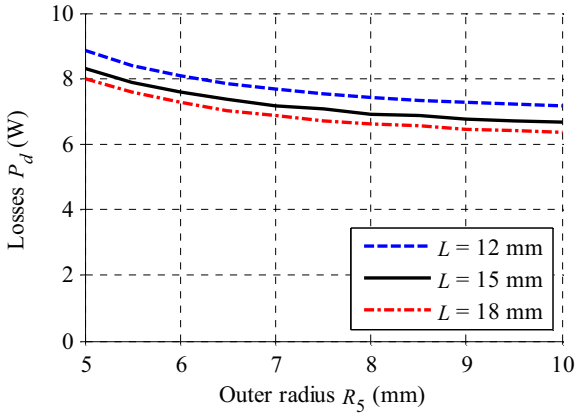

Figure 8. Optimization results for the silicon iron core: total losses P_d for variable outer radius R_5 of the stator core and various values of the core length L . The shaft power is 100 W and the rotational speed 500 000 rpm.

D. *Influence of Stator Core Material*

Figs. 9 and 10 show the loss minimization results when the stator core material was laminated amorphous iron (Metglas magnetic alloy 2605SA1). In this case, the iron losses are lower than 10% of the total losses. If the original outer dimensions of the machine are used, a loss reduction to about 5.2 W is possible by choosing $R_4 = 4.5$ mm and $R_1 = 1.9$ mm . The losses of the existing machine (14.2 W) can thus be reduced by 63% without changing the outer dimensions.

It is obvious that for constant L , the results in Figs. 9 and 10 do not depend much on the outer radius R_5 if $R_5 \approx 6$ mm or larger. Thus the outer diameter of the stator can be reduced from the original value with almost no influence on the losses. The losses are higher at the lowest values of R_5 . The loss increase is caused by two constraints used in the optimization: the minimum thickness of the stator core (1 mm) and the maximum flux density allowed in the stator core (1.1 T). The geometry and the magnetic field plot of the loss-minimizing design are shown in Fig. 11.

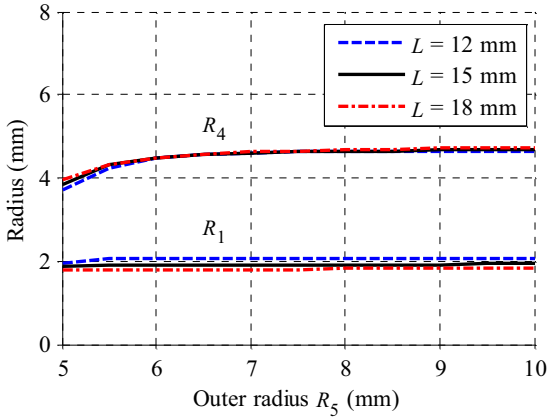

Figure 9. Optimization results for the amorphous iron core: magnet radius R_1 and inner radius R_4 of the stator core for variable outer radius R_5 of the stator core and various values of the core length L. The shaft power is 100 W and the rotational speed 500 000 rpm.

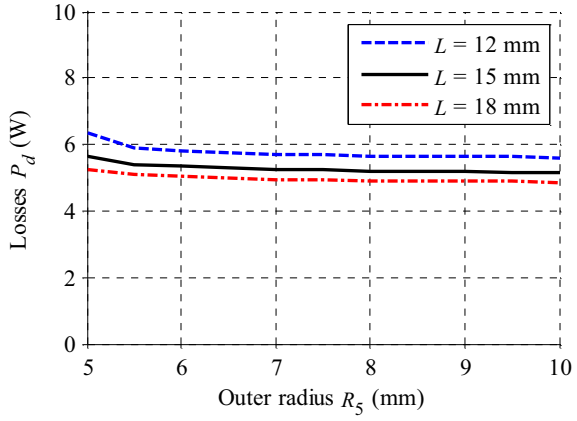

Figure 10. Optimization results for the amorphous iron core: total losses P_d for variable outer radius R_5 of the stator core and various values of the core length L. The shaft power is 100 W and the rotational speed 500 000 rpm.

E. Influence of Air Friction Losses

The air friction losses (16) are approximately proportional to R_2^4. At high speeds, the inclusion of this loss component in the loss minimization leads to a smaller rotor radius than the one obtained without this loss component. This fact is illustrated in Figs. 12 and 13 showing the loss minimization results when the air friction losses are omitted.

F. Influence of Speed

In order to investigate the influence of the rotational speed on the results, the losses of 100-W motors were minimized in the speed range between 100 000 and 1 000 000 rpm. The core length was fixed to $L = 15$ mm, and the outer radius R_5 of the core was adjusted in such a way that the flux density was 1.1 T (if possible without contradicting the minimum core thickness constraint). The results are shown in Figs. 14 and 15. It is obvious that the inclusion of the air friction losses in the loss minimization leads to very small rotor diameters at the highest speeds. For the power rating considered, the analysis of rotor dynamics would have to be included in the optimization for speeds higher than 500 000 rpm, which finally restricts the reduction of the rotor radius with increasing speed.

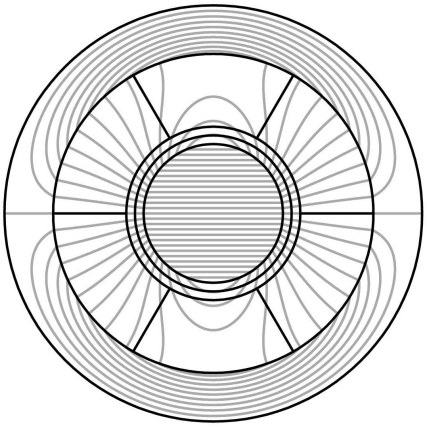

Figure 11. Geometry and field plot of the optimized machine.

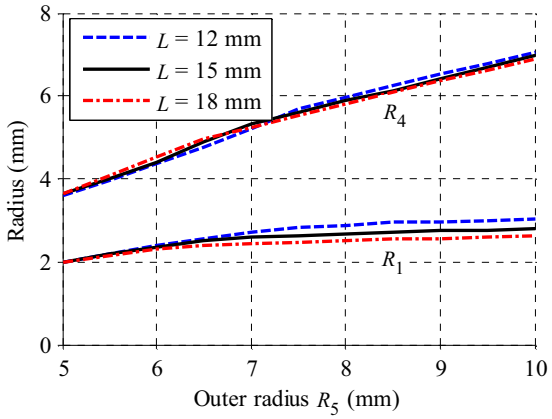

Figure 12. Optimization results when air friction losses are omitted. Explanations of curves are as in Fig. 9.

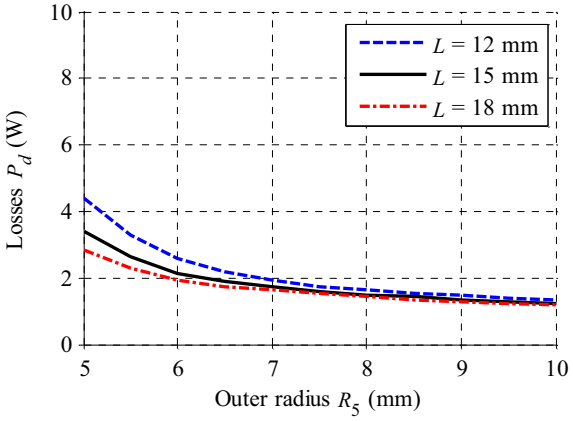

Figure 13. Optimization results when air friction losses are omitted. Explanations of curves are as in Fig. 10.

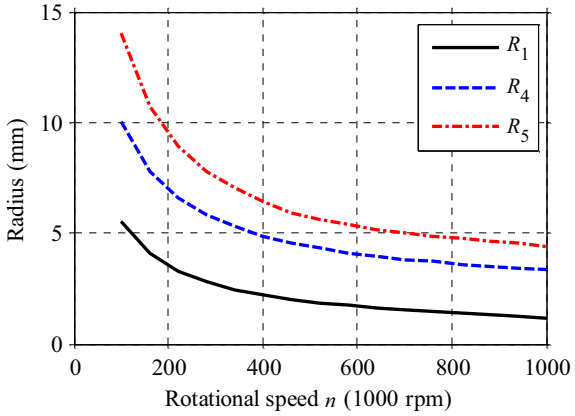

Figure 14. Magnet radius R_1, and inner radius R_4 and outer radius R_5 of the stator core as functions of the rotational speed n used in the optimization. The shaft power is 100 W and the core length $L = 15$ mm.

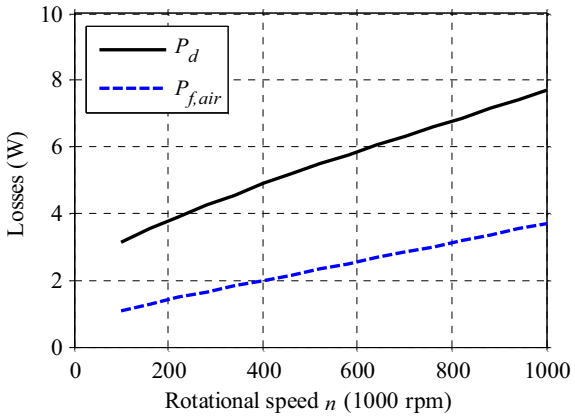

Figure 15. Total losses P_d and air friction losses $P_{f,air}$ as functions of the rotational speed n used in the optimization. The shaft power is 100 W and the core length $L = 15$ mm.

VII. Conclusion

Analytical models can be used for the optimization of high-speed permanent-magnet machines that are equipped with a diametrically magnetized rotor and a slotless stator. In the efficiency optimization of an ultra-high-speed machine, the air friction losses have to be taken into account in addition to the usual iron losses, copper losses, and eddy current losses. In this paper, general analytical models are presented for the field calculation and loss components, and an existing machine design is optimized for efficiency.

The calculated losses of the existing 100-W, 500 000-rpm machine, designed without considering air friction, are 14.2 W. The optimization of the magnet radius and the inner radius of the stator core results in a reduction of the losses by 5.2 W. The minimization of the sleeve thickness and air gap further reduces the losses by 2 W, whereas the improvement by optimizing the already thin litz wire strand diameter is negligible. Changing the core material from silicon iron to amorphous iron laminations decreases the losses by another 1.8 W. The final machine design has 5.2 W total losses, which is 63% lower than those of the existing machine.

It can be concluded that for a loss-minimizing design, the proximity effect losses and the air friction losses have to be taken into account on an ultra-high-speed machine with a slotless stator. The proximity effect loss calculation leads to a litz wire winding with a small strand diameter, and including the air friction losses results in a small magnet radius. In addition to low losses, the use of a high-frequency stator core material—such as amorphous iron—allows for a smaller outer diameter of the stator with an insignificant increase in the total losses.

Going towards 1 000 000 rpm results in machines with decreasing magnet and shaft radii. For designing machines to be integrated into various applications, the efficiency optimization will be coupled with the rotor dynamic and thermal analyses. Results of research in this direction will be published in a future paper.

References

[1] M.A. Rahman, A. Chiba, and T. Fukao, "Super high speed electrical machines – summary," in *2004 IEEE Power Engineering Society General Meeting*, June 6-10, 2004, Vol. 2, pp. 1272-1275.

[2] C. Zwyssig, S.D. Round, and J.W. Kolar, "Analytical and experimental investigation of a low torque, ultra-high speed drive system," in *IEEE Industry Applications Conference 2006, Conference Record of the 41th IAS Annual Meeting*, Tampa, FL, Oct. 8-12, 2006, Vol. 3, pp. 1507-1513.

[3] C. Zwyssig, J.W. Kolar, W. Thaler, M. Vohrer, "Design of a 100 W, 500000 rpm permanent-magnet generator for mesoscale gas turbines," in *IEEE Industry Applications Conference 2005, Conference Record of the 40th IAS Annual Meeting*, Hong Kong, Oct. 2-6, 2005, Vol. 1, pp. 253-260.

[4] J.D. Ede, Z.Q. Zhu, and D. Howe, "Optimal split ratio for high-speed permanent magnet brushless DC motors," in *Proc. Int. Conf. on Electrical Machines and Systems*, Shenyang, China, 2001, pp. 909–912.

[5] N. Bianchi, S. Bolognani, and F. Luise, "Potentials and limits of high-speed pm motors," *IEEE Trans. Ind. Applicat.*, vol. 40, no. 6, pp. 1570-1578, Nov.-Dec. 2004.

[6] Z.Q. Zhu, D. Howe, E. Bolte, and B. Ackermann, "Instantaneous magnetic field distribution in brushless permanent magnet dc motors, Part I: Open-circuit field," *IEEE Trans. Magn.*, vol. 29, no. 1, pp. 124-135, Jan. 1993.

[7] U. Kim and D.K. Lieu, "Magnetic field calculation in permanent magnet motors with rotor eccentricity: Without slotting effect," *IEEE Trans. Magn.*, vol. 34, no. 4, pp. 2243-2252, July 1998.

[8] K.F. Rasmussen, J.H. Davies, T.J.E. Miller, M.I. McGilp, and M. Olaru, "Analytical and numerical computation of air-gap magnetic fields in brushless motors with surface permanent magnets," *IEEE Trans. Ind. Applicat.*, vol. 36, no. 6, pp. 1547-1554, Nov. 2000.

[9] Z.Q. Zhu, D. Howe, and C.C. Chan, "Improved analytical model for predicting the magnetic field distribution in brushless permanent-magnet machines," *IEEE Trans. Magn.*, vol. 38, no. 1, pp. 229-238, Jan. 2002.

[10] T. Modeer, "On stator yoke rotational iron losses in permanent magnet machines," in *Proc. ICEM 2006*, Chania, Crete Island, Greece, Sept. 2-5, 2006, Paper No. OTA4-1, 5 pp.

[11] L. Atallah, Z.Q. Zhu, D. Howe, and T. Birch, "Armature reaction field and winding inductances of slotless permanent-magnet brushlesss machines," *IEEE Trans. Magn.*, vol. 34, no. 5, pp. 3737-3744, Sept. 1998.

[12] J.A. Ferreira, *Electromagnetic modeling of power electronic converters*. Norwell, Massachusetts: Kluwer Academic Publishers, 1989.

[13] X. Nan and C.R. Sullivan, "An equivalent complex permeability model for Litz-wire windings," in *IEEE Industry Applications Conference 2005, Conference Record of the 40th IAS Annual Meeting*, Hong Kong, Oct. 2-6, 2005, Vol. 3, pp. 2229-2235.

[14] M. Mack, "Luftreibungsverluste bei elektrischen Maschinen kleiner Baugrösse," Ph.D. Dissertation, Universität Stuttgart, Germany, 1967.

[15] Pack Feindrähte, Litz wire table, Available: http://www.pack-feindraehte.de, May 2, 2007.